Magnetic excitations and orbital physics in the ferrimagnetic spinels MnB_2O_4 (B=Mn,V)

J.-H. Chung
NIST Center for Neutron Research, National Institute of Standards and Technology, Gaithersburg, Maryland 20899-8552, USA and Department of Physics, Korea University, Seoul 136-713, Republic of Korea

J.-H. Kim and S.-H. Lee
Department of Physics, University of Virginia, Charlottesville, Virginia 22904, USA

T. J. Sato
Institute for Solid State Physics, University of Tokyo, Kashiwa, Chiba 277-8581, Japan

T. Suzuki, M. Katsumura, and T. Katsufuji
Department of Physics, Waseda University, Tokyo 169-8555, Japan
(Received 22 October 2007; published 8 February 2008)

Using neutron scattering techniques, we have investigated spin wave excitations in noncollinear ferrimagnetic spinels MnB_2O_4 (B=Mn,V) with e_g and t_{2g} orbital degeneracies, respectively, that lead to tetragonal distortions along opposite directions. Linear spin wave analysis of the excitations yields spatially inhomogeneous nearest neighbor interactions in both tetragonal spinels. We find the ratio $J^c/J^{ab} \approx -0.06(4)$ for Mn_3O_4 ($c>a=b$) and $\approx 0.3(1)$ for MnV_2O_4 ($c<a=b$). Resulting exchange couplings of Mn_3O_4 can be qualitatively explained in terms of possible overlaps of t_{2g} and e_g electrons of Mn^{2+} and Mn^{3+} ions. On the other hand, those of MnV_2O_4, in particular, the strong J^c, seem to contradict with the antiferro-orbital state of V^{3+} (t_{2g}^2) ions that was proposed by a recent synchrotron x-ray study [T. Suzuki *et al.*, Phys. Rev. Lett. **98**, 127203 (2007)]. Theoretical implications to the orbital physics are also discussed.

DOI: 10.1103/PhysRevB.77.054412 PACS number(s): 75.30.Et, 75.30.Ds, 75.50.Gg

I. INTRODUCTION

In strongly correlated spin systems, the electronic orbital degree of freedom can play a central role in inducing novel low temperature phenomena. This is because the effective Hamiltonian for magnetic interactions, which is originated from the Coulomb interactions and the Pauli's exclusion principle, is determined by the spatially overlapping electronic orbitals. When the orbital degree of freedom is degenerate, it can couple to the lattice, called Jahn-Teller distortion, and induces a phase transition into an orbitally ordered state. Such an orbital ordering can dramatically affect the magnetic properties of the system. Colossal magnetoresistive manganites are good examples where strong orbital correlations play a crucial role in the antiferromagnetic insulator-to-ferromagnetic metal transition.[2] When the spin degree of freedom is also degenerate, a plethora of complex states can emerge out of interactions between the spin, orbital, and lattice degrees of freedom.

Vanadate spinels, AV_2O_4, provide ideal systems to study such complex orbital phenomena because the magnetic V^{3+} ions with t_{2g} orbital degeneracy are located at vertices of a network of corner-sharing tetrahedra that is magnetically frustrating. Even without orbital degeneracy, the spinels exhibit rich physics at low temperatures. For instance, in ACr_2O_4 (A=Zn,Cd,Hg; Cr^{3+}:$t_{2g}^3e_g^0$), a spin-lattice coupling transition occurs to lift the spin degeneracy that leads simultaneously to a long range magnetic order and a cubic-to-tetragonal distortion.[3–5] The one-to-one correspondence of the selected spin structure and the lattice distortion has recently been revealed in $HgCr_2O_4$.[5] When there is orbital degeneracy as in AV_2O_4, the additional orbital degeneracy leads to more than one phase transition at low temperatures.[6,7] So far, several theoretical models were proposed in attempts to explain the physics of vanadates. Vanadates with t_{2g} degeneracy as in $A^{2+}V^{3+}O_4$ (V^{3+}:$t_{2g}^2e_g^0$) usually undergo a contraction along the c axis, which favors the d_{xy} orbital to be occupied by a t_{2g} electron of every V^{3+} ion. The second t_{2g} electrons, however, can either occupy different d_{yz} and d_{zx} orbitals alternatingly along the c axis [*antiferro-orbital*, see Fig. 1(a) in Ref. 9],[8] occupy the same $d_{yz} \pm id_{zx}$ [*ferro-orbital*, see Fig. 1(b) in Ref. 9],[9] or form a more complex pattern.[10] While all these models lead to orbital and/or spin chains of d_{xy} in the ab planes, the interchain couplings between the neighboring ab planes are expected to be considerably different: for instance, the interchain coupling will be much weaker in the antiferro-orbital state than in the ferro-orbital state. Experimental indications of such weakly interacting spin chains have been observed by inelastic neutron scattering measurements on powder samples of AV_2O_4 [A=Zn (Ref. 7), Cd (Ref. 11)]. Due to the intrinsic powder averaging in the neutron scattering intensity, they provide limited information regarding which particular orbital state is realized in which vanadate.

In this paper, we report our elastic and inelastic neutron scattering measurements on single crystals of a related vanadate, MnV_2O_4. Upon cooling, MnV_2O_4 undergoes a magnetic long range ordering near 60 K and a cubic-to-tetragonal distortion follows at a lower temperature, 58 K, at which another magnetic ordering occurs simultaneously.[12,13] We have measured dispersion relations of the magnetic excitations at 5 K and have performed linear spin wave calculations to extract exchange couplings. Our results show spatially inhomogeneous pattern of the B-B exchange couplings, in which the strengths of the corresponding pairwise exchange interactions depend on the direction of the bond. For

instance, the exchange between orbital chains, $J'_{BB} \equiv J^c$, is weaker but still has a considerable strength in comparison with the exchange along the chains, $J_{BB} \equiv J^{ab}$, and their ratio is $J'_{BB}/J_{BB} \sim 0.3(1)$. This is surprising because a recent synchrotron x-ray study indicated that this system has the antiferro-orbital state below 58 K that would yield much weaker J'_{BB}.[1] Our results imply that the orbital correlations in MnV_2O_4 might be more complex than the simple antiferro-orbital order. In comparison, we have also investigated spin wave excitations in another related spinel Mn_3O_4 that has e_g orbital degeneracy and undergoes an elongation along the c axis. The obtained coupling constants could be qualitatively understood with conventional direct overlaps of t_{2g} orbitals and superexchange interaction paths involving e_g orbitals.

II. EXPERIMENT

High quality single crystal samples of Mn_3O_4 and MnV_2O_4, each weighing ≈ 1 gram, were grown by the floating zone method. Regardless of cubic-to-tetragonal distortions, we maintain the face-centered unit cell ($a=b\approx c$) for simplicity of discussions. The neutron scattering experiments were performed using two triple axis spectrometers at NIST Center for Neutron Research. Most of the inelastic scattering measurements were done at the BT9 thermal neutron spectrometer. The pyrolytic graphite analyzer was fixed to select $E_f=14.7$ meV and a series of horizontal collimators, 40′-47′-80′-120′, were used in the order following the neutron flight path. The resulting instrumental energy resolution was ≈ 1.7 meV in full width at half maximum at $\hbar\omega=0$. A pyrolitic graphite filter was inserted to remove higher order contaminations in the scattered beams. The temperature dependence of the Bragg peaks and high resolution inelastic data were measured at the SPINS cold neutron spectrometer. The analyzer was fixed to select $E_f=5.0$ meV and the collimator sequence was guide 80′-80′ open. The Be filters were used to remove higher order contaminations.

III. RESULTS AND DISCUSSION

A. Magnetic structures and phase transitions of MnV_2O_4 and Mn_3O_4

Temperature dependence of magnetic Bragg peak intensities [Fig. 1(a)] demonstrates the complex nature of magnetic transitions in MnV_2O_4. As the material is cooled down from the cubic paramagnetic phase, a collinear Néel-type ferrimagnetic (FIM) order sets up at $T_N \approx 61$ K as indicated by a slow rise of (202) intensity in a good agreement with the bulk magnetization.[12] As the temperature is further decreased below $T_{YK}=58$ K, magnetic (200) intensity starts to increase rapidly. This is consistent with the previous neutron powder diffraction data,[13] indicating a transition to a noncollinear Yafet-Kittel (YK)-type FIM structure shown in Fig. 1(c).[14] Such two-step transition is ascribed to the geometrical frustration among antiferromagnetic interactions between the nearest neighbor V^{3+} ions. It has been shown that the noncollinear FIM is not stable under the cubic symmetry when only the nearest neighbor Heisenberg exchanges are considered.[15] Indeed, the cubic-to-tetragonal distortion occurs simultaneously at T_{YK} where the noncollinear FIM structure is finally stabilized [Fig. 1(b)].

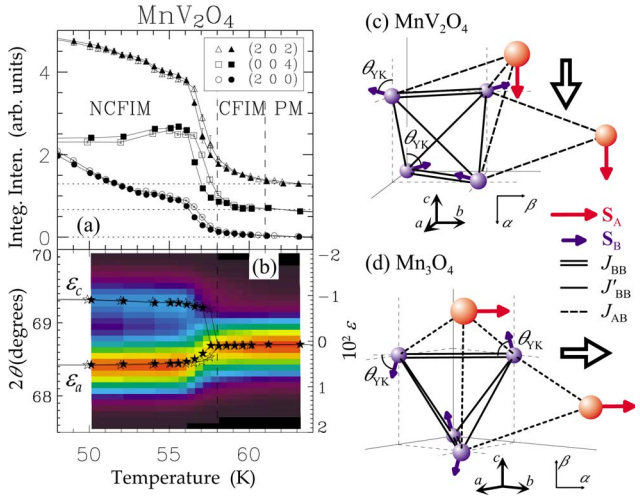

FIG. 1. (Color online) (a) Integrated intensities of three Bragg peaks near the magnetic and structural phase transitions. The empty (filled) symbols are measured during warming (cooling). The relative intensities and backgrounds are arbitrary. PM, CFIM, and NCFIM correspond to paramagnetic, collinear ferrimagnetic, and noncollinear ferrimagentic phases, respectively. (b) Contour map of the (004) Bragg peak intensity. Overplotted is the lattice strain calculated from scattering angles. (c) and (d) Magnetic structures and exchange interactions in noncollinear FIM phases of (c) MnV_2O_4 and (d) Mn_3O_4. The large empty arrows show the directions of net moment.

In comparison, Mn_3O_4 that is already in a tetragonal phase does not show a collinear Néel order but directly orders into noncollinear FIM structures at 42 K.[16] Figures 1(c) and 1(d) show how the spins at the A sites ($\mathbf{S}_A$) and those at the B sites ($\mathbf{S}_B$) are oriented among themselves in MnV_2O_4 and Mn_3O_4, respectively. Although the two spin structures may look different at a glance, they, in fact, are nearly equivalent to each other. In both structures, two neighboring $\mathbf{S}_B$'s located in the same ab plane are separated by an angle $2\theta_{YK}$, and their sum is antiparallel to $\mathbf{S}_A$.[16] As a result, the direction of total magnetization is parallel to $\mathbf{S}_A$, which lies within the ab plane for $B=Mn^{3+}$ and is along the c axis for V^{3+}. More importantly, the spin structure of Mn_3O_4 can be transformed into that of MnV_2O_4 by uniformly rotating all spins together, except the difference in their values of θ_{YK}.[14] This suggests qualitative similarities between magnetic exchange interactions in the two spinels, despite their tetragonal distortions occurring in the opposite directions.

B. Magnetic exchange interactions in Mn_3O_4

In order to reveal the quantitative nature of the magnetic exchange couplings in the two systems, we have performed inelastic neutron scattering measurements in their noncollinear FIM phases. We first present the results from Mn_3O_4 because its excitation spectra are simpler and can provide us with important clues to the interpretation of the excitation spectra in MnV_2O_4.

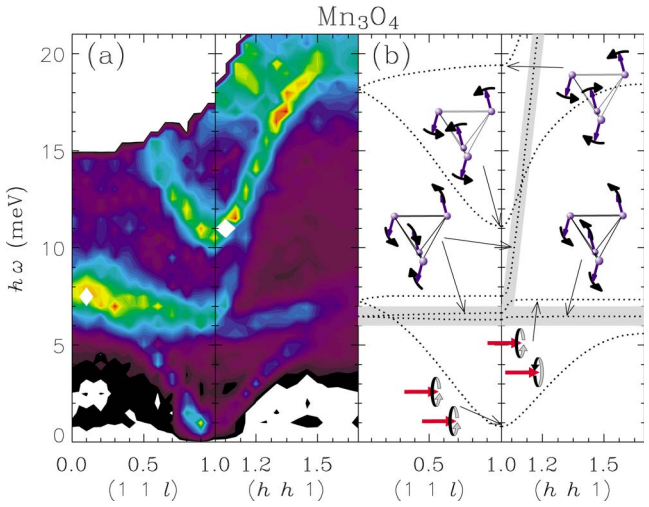

FIG. 2. (Color online) (a) The inelastic neutron scattering intensity from the noncollinear FIM phase of Mn_3O_4 at 5 K. The intensity contour was multiplied by the frequency to enhance the upper band. (b) Calculated spin wave dispersions and polarizations based on the simplified spin structure shown in Fig. 1(b). The black arrows drawn for the two highest modes indicate the displacements within the $\alpha\beta$ plane, while those for the two intermediate (middle) modes indicate perpendicular to the plane. The used parameters are listed in Table I.

Figure 2(a) shows the inelastic neutron scattering spectra obtained from Mn_3O_4 at 5 K along two high symmetry directions. There are several observable modes that can be categorized into two bands. The lower energy band below 10 meV consists of the lowest energy dispersive mode with a gap $\Delta=1.0$ meV and nearly flat modes around ≈ 7 meV. The high energy band above 10 meV also consists of dispersive and nearly flat modes. In addition, there is a strongly anisotropic mode above 5 meV that is steeply dispersive along $(h,h,1)$ and is nearly flat along the c axis.

In order to identify the observed modes and quantitatively understand the exchange interactions, we have performed the linear spin wave calculations based on the Holstein-Primakoff formalism.[17] The magnetic Hamiltonian may include the isotropic Heisenberg exchange constants J_{ij} and the single ion anisotropies D_i^d, where d is the axis of the anisotropy. Since the sizes of the ordered moments are different between the A and the B sites ($S_A \neq S_B$) in the FIM phase, we define $\tilde{J}_{ij}=S_iS_jJ_{ij}$ and $\tilde{D}_i=S_i^2D_i$ so that the spin Hamiltonian can be written in a simple form as follows:

$$\mathcal{H}=-\frac{1}{2}\sum_{i\neq j}\tilde{J}_{ij}\hat{\mathbf{s}}_i\cdot\hat{\mathbf{s}}_j+\sum_{i,d}\tilde{D}_i^d(\hat{s}_i^d)^2, \quad (1)$$

where $\hat{\mathbf{s}}_i$ is a unit spin vector at site i. The simplest Hamiltonian that gives reasonable fits to the data include the nearest neighbor exchange interactions between A and B ions ($\tilde{J}_{AB}$), those between B ions ($\tilde{J}_{BB}$, $\tilde{J}'_{BB}$), and single ion anisotropies for both ions. During calculations, the orientations of B ion spins were adjusted to minimize the magnetic mean-field energy by a relation $\cos(\theta_{YK})=3\tilde{J}_{AB}/(2\tilde{J}_{BB}+2\tilde{J}'_{BB}+\tilde{D}_B^{\alpha}-\tilde{D}_B^{\beta})$. Above, α and β are the directions parallel to $\mathbf{S}_A$ and $(\mathbf{S}_A\times\mathbf{S}_B)\times\mathbf{S}_A$, respectively, so all spins lie on the $\alpha\beta$ plane [see Figs. 1(c) and 1(d)]. The optimal values of the parameters that produce the best fit to the inelastic scattering data are listed in Table I. As shown in Fig. 2(b), the calculated spin waves with the simplified set of parameters reproduce the majority of important features of the data, such as two major bands and the intermediate band that is highlighted by gray shades.

Polarization directions of the spin waves were also calculated and their major components are schematically shown in Fig. 2(b). The two modes of the lower band are due to acoustic (symmetric and lower energy) and optical (antisymmetric and higher energy) oscillations of the $\mathbf{S}_A$ spins. On the other hand, the other four modes involve mostly vibrations of the $\mathbf{S}_B$ spins: the two intermediate energy modes are mainly due to the symmetric (lower energy) and the antisymmetric (higher energy) $\mathbf{S}_B$ oscillations out of the $\alpha\beta$ plane about the axis of $\mathbf{S}_A$, while the upper energy modes are due to their symmetric (lower energy) and antisymmetric (higher energy) oscillations within the $\alpha\beta$ plane. Among the two intermediate energy modes, the polarization of the lower mode that is nearly dispersionless at ≈ 7 meV involves mostly the antiferromagnetic components of the $\mathbf{S}_B$, which are subject to a geometrical frustration. Therefore, it corresponds to the zero energy mode of an antiferromagnetic B-site spinel[4] that is lifted in energy by a single ion anisotropy of $\tilde{D}_B^z=-0.28(3)$ meV. On the other hand, the energy splitting between the two intermediate modes at the zone center is proportional to the strength of J'_{BB}. It is because J'_{BB} is canceled for the lower mode due to its antiferromagnetic oscillation, while it remains uncanceled for the upper mode depending on the direction of the wave propagation. For Mn_3O_4, our linear spin wave calculations yield $J'_{BB}/J_{BB}=-0.06(4)$, indicating that the exchange between Mn^{3+} spins between adjacent ab planes are weak and ferromagnetic (see Table I). The

TABLE I. The optimal parameters used to calculate spin wave dispersions of Mn_3O_4 [Fig. 2(b)] and MnV_3O_4 (Fig. 3) ($\tilde{J}$ and $\tilde{D}$ are in meV).

	$\tilde{J}_{AB}$	$\tilde{J}_{BB}$	$\tilde{J}'_{BB}$	$\tilde{D}_A^{1\bar{1}0}$	$\tilde{D}_B^z$	
Mn_3O_4	2.7(1)	19(1)	−1.1(7)	−0.1(3)	−0.28(3)	
	$\tilde{J}_{AB}$	$\tilde{J}_{BB}$	$\tilde{J}'_{BB}$	$\tilde{D}_A^z$	$\tilde{D}_B^y$	$\tilde{D}_B^z$
MnV_2O_4	2.8(2)	9.8(9)	3.0(8)	−0.6(4)	−4.0(4)	2.7(9)

small ratio J'_{BB}/J_{BB} can be understood when the tetragonal distortion that involves a huge elongation along the c axis ($c/a=1.16$) is considered. The magnetic interactions between Mn^{3+} ($t_{2g}^3 e_g^1$) ions mainly come from two contributions: one from the direct overlap of neighboring t_{2g} orbitals, which is strongly antiferromagnetic and is very sensitive to the distance between the ions, and the other from the superexchange interaction involving neighboring e_g electrons and oxygen's $2p$ electrons, which is very weakly ferromagnetic due to the bond angle of $\approx 90°$. For J_{BB} that is in the ab plane, the overlap contribution is dominant. For $J_{BB'}$ that is out of the ab plane, on the other hand, the direct overlap contribution becomes small because of the c-axis elongation and the ferromagnetic superexchange interaction becomes relevant. These can qualitatively explain the experimentally determined exchange constants for Mn_3O_4 that are listed in Table I.

C. Magnetic exchange interactions in MnV_2O_4

Since the magnetic structures and the magnetic Hamiltonians are essentially similar between MnV_2O_4 and Mn_3O_4, the qualitative nature of the spin wave modes is expected to be similar between the two systems. Figures 3(a) and 3(b) show the spin wave excitations obtained from a single crystal of MnV_2O_4 at 5 K ($c<a$). There are two energy bands, similar to the case of Mn_3O_4. The lower band is mostly due to the magnetic fluctuations of Mn^{2+} ($S=5/2$), thus showing very similar behavior as in Mn_3O_4. On the other hand, the upper band is mostly due to the fluctuations of the V^{3+} ($S=1$) ions shows very different behaviors from the corresponding band of Mn_3O_4. For instance, all of the four modes appear above ≈ 17 meV, making those modes well separated from the lower Mn^{2+} modes. Furthermore, the energy splitting of the two intermediate modes at the zone center is about 5 meV, indicating a stronger J'_{BB} in MnV_2O_4 than in Mn_3O_4. We note that the experimentally observed spin wave spectra in MnV_3O_4 are much more complicated than those in Mn_3O_4 because of the presence of crystallographic as well as magnetic domains due to the pseudocubic crystal lattice. However, the spin wave energies at high symmetry points, such as zone center and zone boundaries, are not affected by the presence of the domains. The optimal exchange parameters that best reproduce the inelastic scattering data of MnV_2O_4 are summarized in Table I, and the calculated dispersions are plotted as lines in Figs. 3(a) and 3(b). Figures 3(c) and 3(d) show contour maps of the calculated neutron scattering intensities that are convoluted with the instrumental energy resolution, which are in a good agreement with the experimental data.

Our most important result is that the ratio of the in-plane and out-of-plane nearest neighboring B-B interactions for MnV_2O_4 is $J'_{BB}/J_{BB}=0.3(1)$ that is much larger than the ratio for Mn_3O_4, $J'_{BB}/J_{BB}=-0.06(4)$. One might be tempted to say that this difference is due to the different nature of their lattice distortions, i.e., the contraction and the elongation along the axis for MnV_2O_4 and for Mn_3O_4, respectively. The problem, however, becomes more complex when the t_{2g} orbital degrees of freedom in MnV_2O_4 are considered. A recent

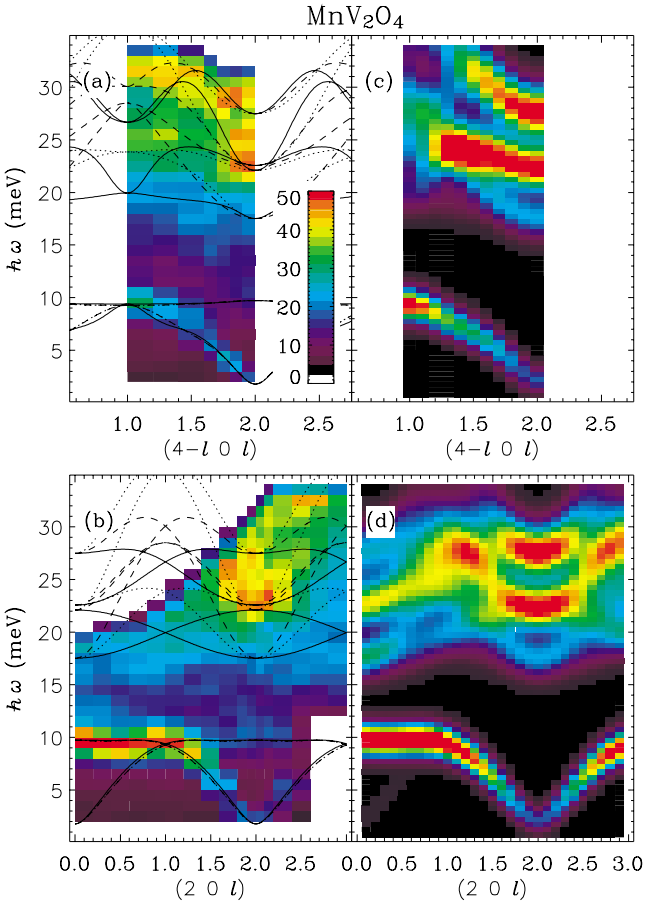

FIG. 3. (Color online) (a) and (b) The contour of inelastic neutron scattering intensity, multiplied by frequency, from the noncollinear FIM phase of MnV_2O_4 at 5 K. In (a) [(b)], the dotted, dashed, and solid lines correspond to dispersions calculated with the parameters listed in Table I along $(0kl)$, $(h0l)$, and $(hk0)$ [$(h00)$, $(0k0)$, and $(00l)$] directions, respectively, which are superposed to be due to the pseudocubic symmetry. (c) and (d) The intensity contour calculated with the optimal parameters and convoluted by energy resolutions.

synchrotron x-ray study of MnV_2O_4 showed that the tetragonal structure of MnV_2O_4 has $I4_1/a$ symmetry, which supports the scenario of the antiferro-orbital ordering.[1] This particular orbital state would yield very weak interchain couplings, $|J'_{BB}/J_{BB}| \ll 1$, because J'_{BB} is due to the negligible overlap between neighboring d_{yz} and d_{zx}, which is supposed to be weakly ferromagnetic according to the Goodenough-Kanamori rules.[18] On the other hand, the ferro-orbital model where the $d_{yz} \pm i d_{zx}$ orbital is occupied by the second t_{2g} electron would yield antiferromagnetic and considerably strong J'_{BB}, which seems to be consistent with our result. However, the ferro-orbital state would have the $I4_1/amd$ tetragonal symmetry, which is inconsistent with the x-ray data.[1] What do these two seemingly conflicting experimental results tell us? It might indicate that the orbital states of V^{3+} ions in the tetragonal MnV_2O_4 are more complex than the two orbital states described above. The ferro- and antiferro-orbital modes have not taken into account the fact that the VO_6 octahedron is trigonally distorted even in the cubic

phase of spinels. In MnV_2O_4, the trigonal distortion is the most severe among vanadates and the octahedron has two different O–O bond lengths: 2.688 and 3.017 Å. It has been shown by *ab initio* local density approximation calculations that a similar trigonal distortion in the cubic phase of a related vanadate, LiV_2O_4, can split t_{2g} orbitals into a singlet and a doublet that are linear combinations of d_{xy}, d_{yz}, and d_{zx}.[19] A similar complex orbital state might be realized in MnV_2O_4 even though its tetragonal distortion ($c<a$) will certainly favor d_{xy}. Such an orbital energy level scheme may account for the seemingly conflicting experimental results. The trigonal distortion may also lead to non-neglibible further neighbor interactions that are not considered in this work using the minimal number of parameters only. Since the interaction beyond the nearest neighbor should involve exchanges through oxygen $2p$ orbitals, the distortions in the VO_6 octahedra will certainly affect the relevant orbital overlaps. This could contribute to an overestimate of the exchange strength between the orbital chains across the c axis. Fully understanding the actual orbital states of vanadates requires *ab initio* calculations based on the first principles on these compounds.

After the submission of this paper, we learned that a new magnetic structure was proposed by Garlea *et al.*,[20] where the antiferromagnetic components of the V^{3+} spins are staggered along the c axis. We note that calculated spin wave energies are similar between the model used in this paper and the one proposed by them. On the other hand, the agreement in the spin wave intensity is substantially better with the former model.

IV. SUMMARY AND CONCLUSIONS

In summary, we have measured spin wave excitations using neutron scattering and determined the effective spin Hamiltonians for MnB_2O_4 (B=V,Mn) in their noncollinear ferrimagnetic phases. In spite of the tetragonal distortions occurring in the opposite directions, the exchange interaction strength between magnetic B-site ions was always stronger in the ab plane (J_{BB}) than between the planes (J'_{BB}). The ratio between these two constants in MnV_2O_4, $J'_{BB}/J_{BB}=0.3(1)$, suggests that the orbital state of MnV_2O_4 may not be explained by the simple antiferro-orbital model. The microscopic spin Hamiltonian obtained for MnV_2O_4 provides a strict test for theoretical models for the orbital physics of vanadates.

ACKNOWLEDGMENTS

The work at SPINS is based on activities supported by the National Science Foundation under Agreement No. DMR-0454672. The work at UVA is supported by U.S. DOE through DE-FG02-07ER45384.

[1] T. Suzuki, M. Katsumura, K. Taniguchi, T. Arima, and T. Katsufuji, Phys. Rev. Lett. **98**, 127203 (2007).
[2] Y. Tokura and N. Nagaosa, Science **21**, 462 (2000).
[3] S.-H. Lee, C. Broholm, T. H. Kim, W. Ratcliff II, and S.-W. Cheong, Phys. Rev. Lett. **84**, 3718 (2000).
[4] J.-H. Chung, M. Matsuda, S.-H. Lee, K. Kakurai, H. Ueda, T. J. Sato, H. Takagi, K.-P. Hong, and S. Park, Phys. Rev. Lett. **95**, 247204 (2005).
[5] M. Matsuda, H. Ueda, A. Kikkawa, Y. Tanaka, K. Katsumata, Y. Narumi, T. Inami, Y. Ueda, and S.-H. Lee, Nat. Phys. **3**, 397 (2007).
[6] M. Onoda and J. Hasegawa, J. Phys.: Condens. Matter **15**, L95 (2003).
[7] S.-H. Lee, D. Louca, H. Ueda, S. Park, T. J. Sato, M. Isobe, Y. Ueda, S. Rosenkranz, P. Zschack, J. Íñiguez, Y. Qiu, and R. Osborn, Phys. Rev. Lett. **93**, 156407 (2004).
[8] H. Tsunetsugu and Y. Motome, Phys. Rev. B **68**, 060405(R) (2003).
[9] O. Tchernyshyov, Phys. Rev. Lett. **93**, 157206 (2004).
[10] D. I. Khomskii and T. Mizokawa, Phys. Rev. Lett. **94**, 156402 (2005).
[11] Z. Zhang, Despina Louca, A. Visinoiu, S.-H. Lee, J. D. Thompson, T. Proffen, A. Llobet, Y. Qiu, S. Park, and Y. Ueda, Phys. Rev. B **74**, 014108 (2006).
[12] K. Adachi, T. Suzuki, K. Kato, K. Osaka, M. Takata, and T. Katsufuji, Phys. Rev. Lett. **95**, 197202 (2005).
[13] R. Plumier and M. Sougi, Solid State Commun. **64**, 53 (1987); Physica B **155**, 315 (1989).
[14] Y. Yafet and C. Kittel, Phys. Rev. **87**, 290 (1952).
[15] T. A. Kaplan, Phys. Rev. **119**, 1460 (1960).
[16] G. B. Jensen and O. V. Nielsen, J. Phys. C **7**, 409 (1974). The magnetic structure of Mn_3O_4 shows a unit cell doubling within the ab plane. However, the model Hamiltonian discussed in the text gives equal magnetic energies and spin wave frequencies between the two nonequivalent cells.
[17] T. Holstein and H. Primakoff, Phys. Rev. **58**, 1098 (1940).
[18] J. B. Goodenough, *Magnetism and the Chemical Bond* (Interscience, New York, 1963); J. Kanamori, J. Phys. Chem. Solids **10**, 87 (1959).
[19] V. I. Anisimov, M. A. Korotin, M. Zölfl, T. Pruschke, K. Le Hur, and T. M. Rice, Phys. Rev. Lett. **83**, 364 (1999).
[20] V. O. Garlea, R. Jin, D. Mandrus, B. Roessli, Q. Huang, M. Miller, A. J. Schultz, and S. E. Nagler, arXiv:0711.1844v1, Phys. Rev. Lett. (to be published).

Erratum: Magnetic excitations and orbital physics in the ferrimagnetic spinels MnB_2O_4 (B = Mn, V) [Phys. Rev. B 77, 054412 (2008)]

J.-H. Chung, J.-H. Kim, S.-H. Lee, T. J. Sato, T. Suzuki, M. Katsumura, and T. Katsufuji

(Received 24 April 2013; published 29 April 2013)

DOI: 10.1103/PhysRevB.87.139907 PACS number(s): 75.30.Et, 75.30.Ds, 75.50.Gg, 99.10.Cd

In this paper, we calculated the linear spin wave energies using incorrectly normalized exchange constants such that $\tilde{J}_{ij} = S_i S_j J_{ij}$ and $\tilde{D}_i = S_i^2 D_i$. In this Erratum we provide the results of our revised analysis, but also argue that the main conclusion of the original paper is still intact. First, the correct way for normalization should have been $\tilde{J}_{ij} = \sqrt{S_i S_j} J_{ij}$ and $\tilde{D}_i = S_i D$, respectively, since the spin wave frequency is proportional to S. The best-fit values of the exchange constants given in Table I of the original paper thus correspond to $\tilde{J}_{ij} = \sqrt{S_i S_j} J_{ij}$ or $\tilde{D}_i = S_i D$, respectively.

The above treatment in fact still ignores the cross terms that occur between different spin moments. To clarify this issue, we performed new calculations without using normalization. The spin moments were explicitly fixed to be $S_A = \frac{5}{2}$ and $S_B = 2$ (for Mn_3O_4) or 1 (for MnV_2O_4). The new parameters are summarized in Table I, which replaces Table I of the original paper. The dispersions and intensities calculated using the new parameters for MnV_2O_4 are summarized in the revised Fig. 3, which replaces Fig. 3 of the original paper. The new results for Mn_3O_4 are essentially identical to what was shown in Fig. 2 of the original paper. We note that the new parameters provided in this Erratum are comparable to those shown in the original paper when converted by the corrected normalization. Most importantly, the ratio indicating the spatial anisotropy of the B-B exchange, $J'_{BB}/J_{BB} = 0.3 \pm 0.1$, is equal to the value reported in the original paper. It is thus confirmed that the conclusions of the original paper still stand without any reservations.

TABLE I. The best-fit parameters used to calculate spin wave energies and intensities of Mn_3O_4 and MnV_2O_4 (J and D are in meV).

	J_{AB}	J_{BB}	J'_{BB}	$D_A^{1\bar{1}0}$	D_B^z	
Mn_3O_4	1.10 ± 0.04	7.8 ± 0.5	-0.4 ± 0.1	-0.05 ± 0.07	-0.17 ± 0.03	
	J_{AB}	J_{BB}	J'_{BB}	D_A^z	D_B^y	D_B^z
MnV_2O_4	1.8 ± 0.2	10.2 ± 0.9	3.0 ± 1.0	-0.1 ± 0.3	-4.8 ± 0.5	0.7 ± 1.3

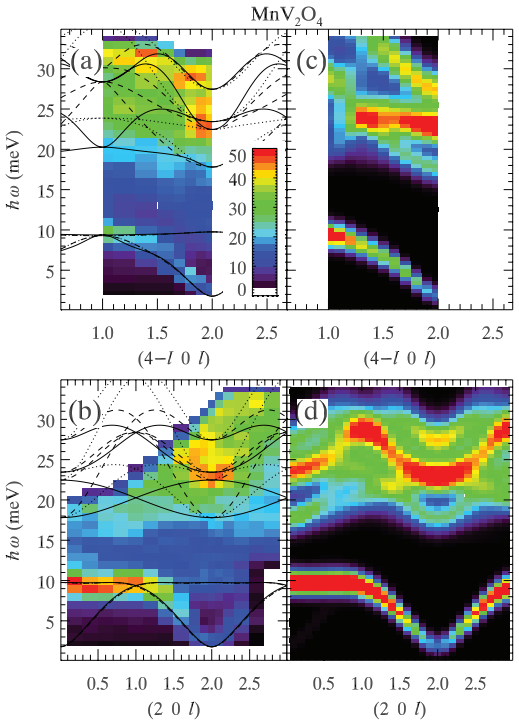

FIG. 3. (Color online) Corrected version of Fig. 3 in the original paper. The experimental data are unchanged, whereas the calculations are done using the new parameters listed in Table I.

